Investigation of oscillating airfoil shock phenomena

Daniel Giordano, Sanford Fleeter

Classification
Physics Abstracts
47.40K — 47.60 — 47.80

Investigation of oscillating airfoil shock phenomena

Daniel D. Giordano and Sanford Fleeter

Thermal Sciences and Propulsion Center, School of Mechanical Engineering, Purdue University, West Lafayette, Indiana 47907, U.S.A.

(Received 13 May 1991, revised 15 October 1991, accepted 17 October 1991)

Abstract. — Fundamental experiments were performed in an unsteady flow water table facility to investigate and quantify the unsteady aerodynamics of a biconvex airfoil executing torsion mode oscillations at realistic reduced frequencies. A computer-based image enhancement system was used to measure the oscillating supersonic and transonic shock flow phenomena. By utilizing the hydraulic analogy to compare experimental results with a linear theoretical prediction, magnitude and phase relationships for the bow shock were determined to be relatively independent of Mach number while the magnitude of oscillation of the shock is a strong function of the reduced frequency. The supersonic bow shock is in phase with the airfoil motion at low reduced frequencies, lagging the airfoil motion as the reduced frequency is increased.

Nomenclature.

a Speed of sound in air, or celerity in water
c wave speed (celerity)
C airfoil chord
d water depth of stream tube
f oscillation frequency, Hertz
Fr freestream Froude number
g acceleration of gravity
h eddying losses in the hydraulic jump
H total head pressure
k reduced frequency, $\omega C/2\,V$
M free-stream Mach number
u flow direction velocity
v normal direction velocity
V free-stream velocity
z water depth
β hydraulic jump angle
γ ratio of specific heats
ω oscillation frequency, radians/s
ρ density
θ wall angle.

SUBSCRIPTS

o stagnation condition
g property in air
w property in water
1 conditions before hydraulic jump or shock wave
2 conditions after hydraulic jump or shock wave.

Introduction.

Recent interest in supersonic and hypersonic flight vehicles has renewed the interest in developing advanced concept propulsion systems such as supersonic axial flow compressors. Since aeroelastic stability in this new flow environment is a concern, mathematical models are being developed to analyze the unsteady aerodynamic loading in supersonic axial flow blade rows. Kielb and Ramsey [1] analyzed the stability characteristics of a supersonic throughflow rotor by developing an oscillating cascade analysis based on the model of Lane [2]. Spara and Fleeter [3] considered the effect of aerodynamic detuning on the torsional mode oscillating airfoil aerodynamics and flutter characteristics of a supersonic axial flow cascade using an approach based on the method of characteristics. However, these are linearized models, with an acoustic shock wave approximation and boundary conditions applied on the mean airfoil position. Thus, such analyses may not model all of the significant flow phenomena. As a result, fundamental unsteady supersonic aerodynamic experimental data are required for model verification and direction.

Supersonic wind tunnel development, cost and time constraints often make it advantageous to study high speed compressible air flow phenomena in water utilizing the hydraulic analogy [4-7]. Other benefits of water table experiments include the ability to observe flow phenomena through normal photographic means without sophisticated equipment, in contrast to a wind tunnel where it is necessary to use holography, interferometry, high speed photography, etc. Also, to investigate the oscillating airfoil and torsional flutter characteristics of an airfoil at realistic high reduced frequencies in a wind tunnel, it is usually necessary to develop a high-speed airfoil drive system. However, due to the different wave speeds in water and air, drive systems to produce realistic reduced frequencies in water operate at much lower oscillatory frequencies.

This paper describes a series of experiments directed at the quantitative investigation of fundamental oscillating airfoil shock phenomena. These experiments utilize an unsteady flow water table in conjunction with computer-based image enhancement to investigate and quantify the fundamental supersonic oscillating airfoil shock flow field phenomena. In particular, for an oscillating airfoil generating bow shocks in a supersonic flow and for an oscillating airfoil with a shock in the midchord region in a transonic flow, the shock motion as a function of the airfoil motion is studied. Also, the instantaneous chordwise location of the normal shock is investigated.

1. Hydraulic analogy.

The similarity between the surface waves produced by ships and those formed by a body moving through air at supersonic speeds was noted as early as 1887 by Mach [8], with the general theory relating the liquid and gas flows developed by Jouquet in 1920 [9]. Black and Mediratta [10] extended the generalized treatment to include the analogy between an hydraulic jump and a normal shock.

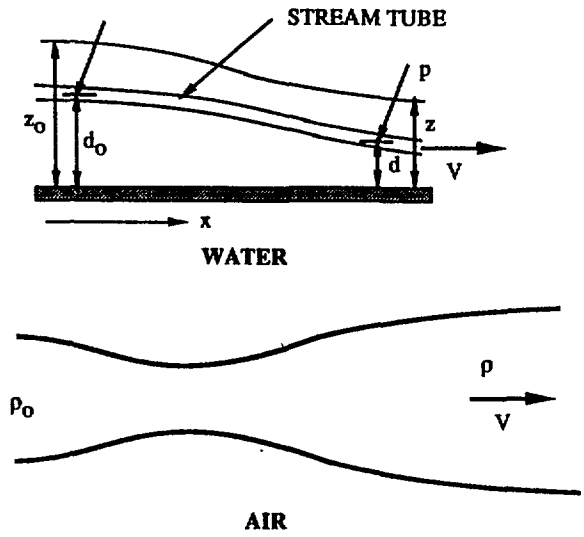

Fig. 1. — Analogy between open channel flow and compressible.

In the development of the main features of the hydraulic analogy, free surface water is assumed to flow over a horizontal channel (if the channel is inclined, then the water velocity is proportional to the sine of the inclination angle), bounded by walls which are similar to those of the corresponding compressible gas flow (Fig. 1). The steady flow hydraulic analogy is obtained by comparing the continuity, momentum, energy, and wave propagation relations for water and for a compressible, inviscid gas.

1.1 CONTINUITY EQUATION. — The continuity equation for two-dimensional water flow is :

$$\frac{\partial(zu)}{\partial x} + \frac{\partial(zv)}{\partial y} = 0 \tag{1}$$

where x and y are the coordinates in and normal to the flow direction, u and v are the corresponding velocity components, and z is the water depth.

For steady two-dimensional gas flow, the continuity equation is :

$$\frac{\partial(\rho_g u)}{\partial x} + \frac{\partial(\rho_g v)}{\partial y} = 0 \tag{2}$$

where ρ_g is the density in the freestream air conditions.

Comparing equations (1) and (2) shows that the water depth, z, corresponds to the gas density, ρ_g.

$$\frac{\rho_g}{\rho_{0g}} \equiv \frac{z}{z_0} \tag{3}$$

where ρ_{0g} is the stagnation density in air and z_0 is the stagnation water level.

1.2 MOMENTUM EQUATION. — Bernoulli's equation for the water stream tube depicted in figure 1 is given in equation (4).

$$p + \frac{1}{2}\rho_w V^2 + \rho_w g z = p_0 + \rho_w g z_0 \tag{4}$$

or

$$V^2 = 2g(d_0 - d) + \frac{2(p_0 - p)}{\rho_w} \tag{5}$$

where d is the water depth, d_0 is the stagnation water level of the centerline of the stream tube, and V is the freestream velocity.

The static pressure at any point in the flow depends only on it's depth below the free surface, that is :

$$p_0 = \rho_w g(z_0 - d_0) \tag{6a}$$

$$p = \rho_w g(z - d) . \tag{6b}$$

Thus from equations (5) and (6) :

$$V^2 = 2 g(z_0 - z) . \tag{7}$$

The maximum velocity the water flow can attain occurs when the water depth, z, is zero

$$V_{max}^2 = 2 g z_0 \tag{8}$$

and

$$\left(\frac{V}{V_{max}} \right)^2 = \frac{(z_0 - z)}{z_0} \tag{9}$$

1.3 ENERGY EQUATION. — The energy equation the flow of a compressible gas is given in equation (10)

$$C_p T + \frac{1}{2} V^2 = C_p T_0 = \frac{1}{2} V_{max}^2 \tag{10}$$

where T is the absolute temperature and C_p is the specific heat at constant pressure. Thus,

$$V^2 = 2 C_p (T_0 - T) \tag{11}$$

and

$$\left(\frac{V}{V_{max}} \right)^2 = \frac{(T_0 - T)}{T_0} \tag{12}$$

From either equations (3) and (11) or equations (9) and (12), it can be seen that the depth ratio in water corresponds to the temperature ratio in the gas

$$\frac{T}{T_0} \equiv \frac{z}{z_0} \tag{13}$$

1.4 EQUATION OF STATE. — The equation of state for the gas is $p = \rho_g RT$. Substituting the equivalent density and temperature relations and the relations for z leads to equation (14). Thus the square of the water depth ratio is equivalent to the gas pressure ratio

$$\frac{p}{p_0} = \left(\frac{\rho}{\rho_0} \right) \left(\frac{T}{T_0} \right) \equiv \left(\frac{z}{z_0} \right)^2 \tag{14}$$

The isentropic pressure-density relation for a gas is $p = K\rho^{\gamma}$ Thus, equation (14) can be written as follows

$$\frac{p}{p_0} = \left(\frac{\rho}{\rho_0} \right)^{\gamma} \tag{15}$$

where γ is the ratio of specific heats.

Comparing equations (3) and (15) shows that for a value of $\gamma = 2$, there is a one-to-one correspondence between the equations describing the water flow and the compressible gas flow, i.e. the water flow may be considered as analogous to an " hydraulic gas " with a ratio of specific heats equal to 2.0.

1.5 WAVE PROPAGATION VELOCITY. — In general, equation (16) defines the velocity of propagation of water surface waves, c [11]

$$c = \left[\left(\frac{g\lambda}{2\pi} + \frac{2\pi\sigma}{\rho\lambda} \right) \tanh \frac{2\pi z}{\lambda} \right]^{1/2} \tag{16}$$

where λ is the wave length and σ is the surface tension.

If the depth, z, is small compared to the wave length, λ, the velocity of propagation of the water surface waves becomes :

$$c = (gz)^{1/2} \tag{17}$$

The capillary waves, represented by the second term in equation (16), thus do not play any part in the hydraulic analogy.

The analogous wave in air is a sound wave, which propagates with velocity a given in equation (18)

$$a = \left(\frac{\gamma p}{\rho g} \right)^{1/2} \tag{18}$$

1.6 FROUDE NUMBER AND MACH NUMBER. — The dynamic similarity criterion for the propagation of water and gas waves is the ratio of the free stream velocity to the wave propagation velocity. Thus, equation (17) leads to the definition of the Froude number for the water flow, equation (19), with the Mach number for the air flow specified in equation (20). Note that when either the Froude number or the Mach number is greater than one, the wave front is the envelope of the circles, in the case of water, or spheres in a gas, the centers of which are convected downstream with velocity V

$$\frac{V}{c} = \frac{V}{(gz)^{1/2}} = \mathrm{Fr} \tag{19}$$

$$\frac{V}{a} = M \tag{20}$$

where Fr is the Froude Number, and M denotes the Mach number.

1.7 DISCONTINUOUS FLOW. — In the flow of either a gas or water, it is possible for a discontinuity to exist. With a gas, the phenomenon is the shock wave which can form when the flow is supersonic. The shock causes an abrupt change in the gas density, temperature, and pressure with a decrease in the velocity also evident. In the case of water flow, the discontinuity is a sudden rise in the depth, termed the hydraulic jump. The hydraulic analogy is summarized in table I. To determine the validity of the hydraulic analogy for supersonic flows, the analogy between these two phenomena is considered.

The hydraulic jump occurs in shooting water. Eddies are produced on the face of the jump resulting in a loss in the " mechanical " energy of the flow (the total energy remains constant, the eddying creating heat cannot be reutilized in liquid flow). The flow through the hydraulic jump is described by equations (21), (22) and (23).

Continuity : $$V_1 z_1 = V_2 z_2 . \tag{21}$$

Momentum : $$\frac{1}{2} g z_1^2 + z_1 V_1^2 = \frac{1}{2} g z_2^2 + z_2 V_2^2 . \tag{22}$$

Energy : $$z_1 + \frac{V_1^2}{(2g)} = z_2 + \frac{V_2^2}{(2g)} + h = H_0 . \tag{23}$$

Table I. — *Summary of hydraulic flow analogy.*

Correlative Characteristic	Free Surface Water Flow	Compressible Perfect Gas Flow
Coordinate System	Quasi-Two Dimensional	Two Dimensional
Energy Equation	$V = \sqrt{2\,g(z_0 - z)}$ $V = \sqrt{2\,gc_p(T_0 - T)}$	$V_{max} = \sqrt{2\,gz_0}$ $V_{max} = \sqrt{2\,gc_p\,T_0}$
Continuity Equation	$\frac{\partial(uz)}{\partial x} + \frac{\partial(vz)}{\partial y} = 0$	$\frac{\partial(u\rho)}{\partial x} + \frac{\partial(v\rho)}{\partial y} = 0$
Wave Propagation	$c_w = \sqrt{gz}$	$a = \sqrt{\gamma RT}$
Velocity Ratio	$\mathrm{Fr} = \frac{V}{\sqrt{gz}}$	$M_\infty = \frac{V}{a}$
Specific Heat Ratio	$\gamma = 2$	$\gamma = 1.4$
Temperature Ratio	$\frac{z}{z_0}$	$\frac{T}{T_0}$
Density Ratio	$\frac{z}{z_0}$	$\frac{\rho}{\rho_0}$
Pressure Ratio	$\left(\frac{z}{z_0}\right)^2$	$\frac{P}{P_0}$
Flow Discontinuity	Hydraulic Jump	Compression Shock
Characteristic Parameter	Froude Number	Mach Number

where the subscripts 1 and 2 represent conditions before and after the hydraulic jump, respectively, h denotes the eddying losses in the jump and H_0, the total head pressure, is the sum of the pressure and kinetic energies.

Utilizing equations (21), (22) and (23), it can be shown that the depth ratio z_2/z_1 is a function of the Froude number

$$\frac{z_2}{z_1} = [(1 + 8(\mathrm{Fr}\ (\sin(\beta)))^2)^{1/2} - 1]/2 \tag{24}$$

where Fr represents the Froude number before the hydraulic jump and β is the wave angle (Fig. 2).

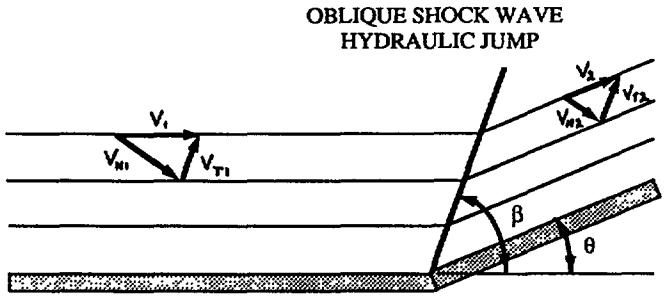

Fig. 2. — Oblique shock geometry.

The analogous equations describing a shock wave in a compressible flow are given in equations (25) through (28).

Continuity
$$\rho_1 V_1 = \rho_2 V_2 . \tag{25}$$

Momentum
$$p_1 + \rho_{g1} V_1^2 = p_2 + \rho_{g2} V_2^2 \tag{26}$$

Energy
$$\frac{1}{2} V_1^2 + \frac{\gamma p_1}{(\gamma - 1)\rho_{g1}} = \frac{1}{2} V_2^2 + \frac{\gamma p_2}{(\gamma - 1)\rho_{g2}} = \frac{\gamma p_0}{(\gamma - 1)\rho_{g0}} = C_p T_0 . \tag{27}$$

Density relation
$$\frac{\rho_2}{\rho_1} = \frac{\frac{1}{2}(\gamma + 1) M_1^2}{1 + \frac{1}{2}(\gamma - 1) M_1^2} \tag{28}$$

Comparing the energy relationships for the hydraulic jump and the shock, equations (23) and (27), it can be seen that the shock losses are not analogous to the hydraulic jump eddying losses, with the shock losses for the gas necessitating the use of the second law as well. Although, the loss in the total head pressure across the shock wave appears to correspond to the same loss in the jump, this is not the case. Namely, the total head pressure, H_0, is a measure of the energy of the water flow whereas it is the total stagnation temperature T_0 which measures the energy of the gas flow. The drop in total stagnation pressure through the shock wave is only an indication of the redistribution of the kinetic, pressure and internal energies of the gas.

Since the energy transport phenomena are different, it is to be expected that the relations derived and verified for continuous flow which were based on analogous energy equations do not apply to discontinuous flow. It follows that depth measurements downstream of an hydraulic jump cannot have the same simple relation to the corresponding gas density measurements downstream of a shock, as would be required by the continuous flow hydraulic analogy, i.e., it is not appropriate to use a gamma of 2.0 in the Rankine-Hugoniot relation to obtain density ratios which agree with those deduced from the measured depths through an hydraulic jump. This is demonstrated in figure 3 which shows a comparison of the flow relations predicted for water and air from equations (24) and (28). If the hydraulic analogy as previously developed for continuous flow was valid, the result for d_2/d_1 *versus* Fr would also represent the density ratio ρ_2/ρ_1 verses Mach number for a shock wave formed in an " hydraulic gas " with a γ of 2.0. However, it is apparent that the curves are not the same. These differences are further illustrated in figure 4 which shows the change in the oblique

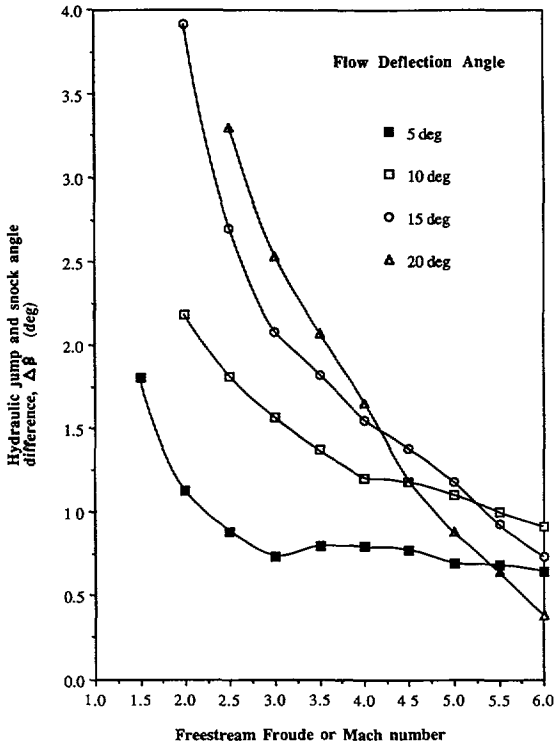

Fig. 3.

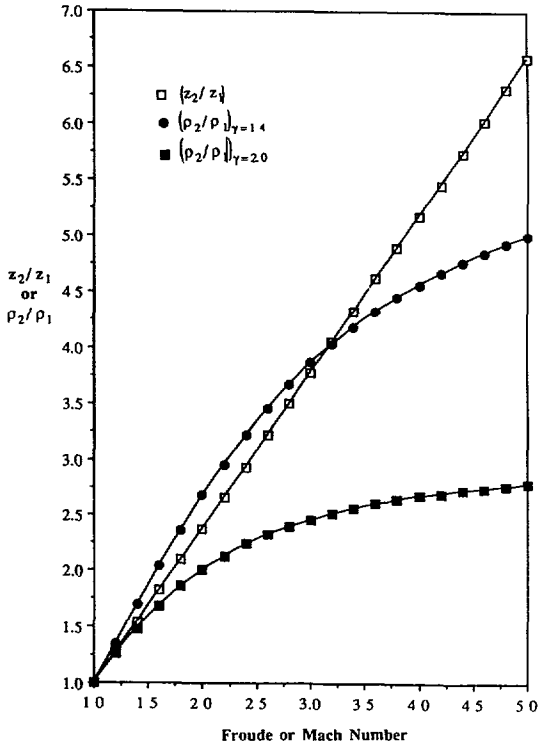

Fig. 4.

Fig. 3. — Comparison of classic hydraulic relations and compressible flow relations for oblique shock.

Fig. 4. — Flow relations across a normal shock wave and hydraulic jump.

shock angle for the hydraulic relations and also for the oblique shock relations with a value of gamma set to 1.4 for flows at equal Mach and Froude numbers, with the wave deflection angle as a parameter. Thus, for an air or water flow with a given inlet Mach or Froude number, the conditions behind the shock or the hydraulic jump are not predicted with the previously derived continuous flow hydraulic analogy. It is therefore necessary to develop a correction to compare the hydraulic jump wave angles with the corresponding compressible gas flow shock angles.

1.8 SHOCK HYDRAULIC ANALOGY CORRECTION. — The shock hydraulic analogy necessary to analyze the data obtained in the water table experiments, thereby leading to the corresponding experimental data for air with a $\gamma = 1.4$ is developed in the following.

For each water table experimental condition, the Froude number is determined by measuring the wall angle, θ, and the hydraulic jump angle, β_w, and iteratively solving equation (29) for the Froude number, Fr

$$\tan \theta = \frac{\tan \beta_w (\sqrt{1 + 8\,\mathrm{Fr}^2 \sin^2 \beta_w - 3})}{(2 \sin^2 \beta_w - 1) + \sqrt{1 + 8\,\mathrm{Fr}^2 \sin^2 \beta_w}} . \tag{29}$$

Once the appropriate Froude number for the experimental condition has been calculated, the airfoil is oscillated through a range of reduced frequencies. At each wall angle, the steady prediction of hydraulic jump angle, β_w, is calculated. Also, the wave angle, β, on the water table is measured.

Since the hydraulic analogy is not correct for flow with hydraulic jumps, setting the Mach number equal to the Froude number results in an error in the correspondence between the depth ratio in water and the gas density ratio. Therefore, for a given Mach number and a wall angle, θ, the aerodynamic relation for an oblique shock, equation (30), is used to determine a quasi-steady aerodynamic prediction of the shock angle, β_g through an iterative process.

$$\frac{1}{\tan\theta} = \left(\frac{\gamma + 1}{2} \frac{M^2}{(M^2 \sin^2 \beta_g - 1)} - 1 \right) \tan \beta_g \,. \tag{30}$$

To correct the wave angle measured from the table, β, to insure a similar condition in air, the difference in water angle, β_w, and gas angle, β_g, is applied to the measured hydraulic jump angle.

2. Water table facility.

The Thermal Sciences and Propulsion Center (TSPC) water table facility used in this experimental investigation, figure 5, is 64.5 in. (163.83 cm) × 46.5 in. (118.11 cm) and is constructed from 3/4 (1.91 cm) plexiglass. The water is driven by a centrifugal pump powered by 2 HP DC electric motor with the test section Froude number continuously variable from 0 to 4. Water flows in a closed loop from the discharge section through the pump, filter, and

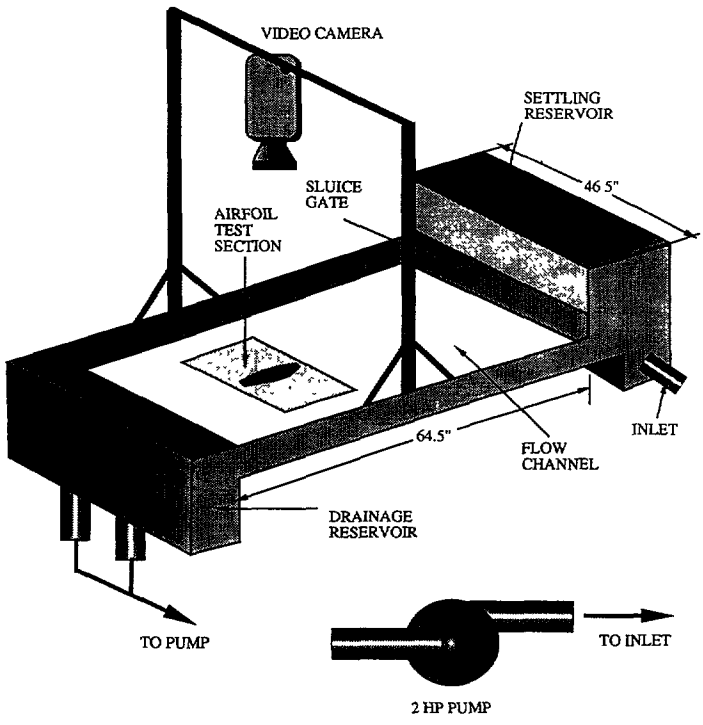

Fig. 5. — Water table facility.

into the settling reservoir. A gate valve between the filter and settling reservoir is also used to control the flow rate. The settling reservoir is filled with open celled polyurethane foam which breaks down the large scale eddies and uniformly distributes the flow across the width of the channel. The water then flows under a sluice gate (nozzle) producing uniform parallel supercritical water flow. This thin uniform shooting water stream passes down the flow channel, through the test section, and into the drainage reservoir completing the circulation cycle.

2.1 AIRFOIL DRIVE SYSTEM. — An airfoil drive system to provide sinusoidal pitching oscillation to the airfoil has been developed. This system consists of a variable speed DC motor and a crank-rod linkage setup which function to transform the circular motion first to reciprocating, and then to airfoil pitch oscillations. The mean angle of airfoil oscillation is controlled by the length of the connecting rods while the amplitude is governed by the radial distance on the crank. This combination of adjustments provides for pitching amplitudes up to +/– 20° about a continuously variable mean angle that ranges from 0° to 20°. The variable crank speed provides oscillation frequencies from 0 to 3 Hz. An optical trigger is mounted on the motor shaft to provide a measure of the oscillation frequency for each experimental condition. Also, an 8-bit rotary encoder provides the instantaneous measurement of the shaft position and, thus, the instantaneous airfoil position.

2.2 AIRFOIL DESIGN. — An uncambered, biconvex airfoil with a chord of 12 in. (30.48 cm) and a thickness-to-chord ratio of 0.076 was used in this study, table II. The radius of curvature of the airfoil surfaces is 43.15 in. (109.60 cm) with leading and trailing edges having a 0.039 in. (0.100 cm) radius of curvature. The airfoil is supported by a midchord trunnion, resulting in a midchord elastic axis.

The airfoil is constructed of three pieces of aluminum in a laminate fashion. First, the core shape of the airfoil was milled by calculating a series of facets along the curvature of the blade in 0.5 degree increments. The rough shape of the airfoil was milled from 2021 aluminum stock on a horizontal milling machine. Since this method of fabrication does not leave an entirely smooth surface, 0.0625 in. (0.1588 cm) thick aluminum sheet was epoxied on each side of the biconvex airfoil and sanded smooth. The leading and trailing edges were then rounded to the correct dimensions, thus completing the fabrication. Torsion rods were fitted to the airfoil by press fitting the 5/16 in. (0.794 cm) diameter rods into predrilled holes. To mount the airfoil in the test section, brass brushings were pressed into holes drilled at the desired geometry location in the test section. Teflon washers were inserted between the bottom of the blade and the test section to provide clearance.

Table II. — *Airfoil geometry.*

Type	Biconvex, no camber
Surface radius of curvature, in (cm)	43.15(109.60)
Leading- and trailing-edge radii of curvature, in (cm)	0.039(0.100)
Thickness, T, in (cm)	0.913(2.32)
Chord, C, in (cm)	12.00(30.48)
Elastic axis	Midchord

3. Data acquisition and analysis.

A computer-based video enhancement system applied to a shadowgraph visualization of the flow field, figure 6 was implemented for quantitative water table data acquisition and

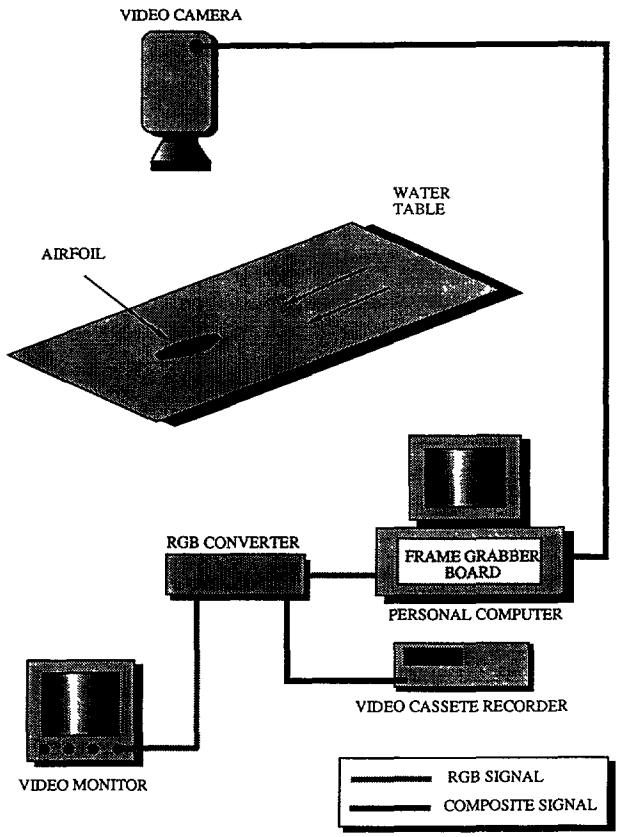

Fig. 6. — Video system schematic.

analysis. To provide the shadowgraph image, a frosted glass sheet is mounted 0.125 in. (0.318 cm) above the airfoil, with the test section illuminated from below with a point light source. The shadowgraph technique depends on the relative deflection of light beams due to variations in the slope of the free channel water surface, with the hydraulic jump appearing as a dark line followed by a light line. This image is recorded by a Panasonic D-5000 video camera and transmitted to a personal computer for digitization and analysis. The computer is equipped with a Data Translation 2851 frame acquisition board and 2858 frame processor. The DT-2851 is a high speed (i.e., real time ~ 30 frames/s) 8 bit, black and white video acquisition board. The video input signal is digitized by a flash A/D converter into 8-bit pixel values with a range of 256 possible gray levels. From the A/D converter, the 8-bit pixel values pass through one of eight user-configurable 256 × 8 bit RAM look up tables (LUT). The LUT converts the various intensity levels to different colors for enhanced comprehension of the flow field. Once the frame has passed through the LUT, it is displayed on a monitor and is also recorded by a video cassette recorder for later playback and analysis.

This video system is configured to provide real time on line acquisition and analysis of the oscillatory airfoil and hydraulic jump motion. Due to the difference in shadow intensity between the airfoil and the flowfield with the shadowgraph technique, the airfoil has been set to appear blue. The background which has a medium intensity level, appears yellow and the shocks (hydraulic jumps) are set to red because of their bright intensity. This color

arrangement provides good recognition of the shock structure and airfoil location for these unsteady experiments.

The instantaneous airfoil angle of attack is determined as follows. The data acquisition windows for the supersonic bow shock and the transonic normal shock experiments are depicted in figures 7 and 8, respectively.

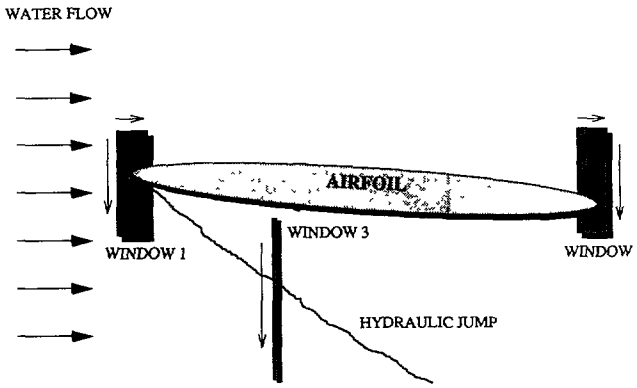

Fig. 7. — Windowing locations for bow shock video data acquisition.

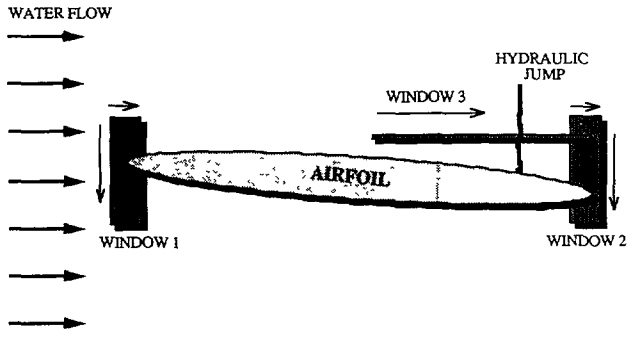

Fig. 8. — Windowing locations for normal shock video data acquisition.

The video processing system provides instantaneous airfoil and hydraulic jump position data. Since the rotary encoder on the airfoil drive system also provides a measure of the instantaneous airfoil oscillation position, each video frame is recorded and analyzed with reference to the encoder position. This allows the measurement of airfoil and hydraulic jump location for an entire oscillation period. As the phenomena of interest is periodic, the limitations in the speed of the video processing system are overcome by analyzing multiple oscillations of the airfoil to determine the airfoil characteristics at each encoder location.

Since the method of analysis is similar for the supersonic and transonic experimental conditions, details of only the supersonic case will be explained. Window 1 of figure 7 is scanned in the direction shown to find the first occurrence of a blue pixel which represents the airfoil leading edge since the color change from the background color of yellow to blue reflects a threshold in intensity level between the airfoil shadow and the background light. In the same manner, Window 2 is scanned and the pixel location of the last blue pixel is

recorded, i.e. the airfoil trailing edge. The airfoil angle of attack for each frame is then calculated since the pixel location from the first window represents the leading edge and the location from the second the trailing edge of the airfoil. The rotary encoder on the motor shaft provides a reference for the video acquisition.

To determine the instantaneous hydraulic jump or shock location, Window 3 is scanned for the first occurrence of a red pixel since the color change from the yellow background to red shows a threshold in intensity level between the background light and the hydraulic jump. When the location has been determined, the angle of the upper and lower shocks (if they exist) are computed since the instantaneous airfoil position has already been determined from the Window 1 and 2 data.

The scanning of video frames occurs at the rate of about 5 frames per second. This is noticeably slower than the real time digitization rate of 30 frames per second board capability due to the time needed for the frame scanning and acquisition of pixel locations representating blade leading and trailing edges and the hydraulic jump location. To obtain a representative sample of data for each angle of attack increment, 1000 frames are sampled. The data obtained for each angle of attack are averaged and the resulting sinusoidal wave data analyzed by Fast Fourier Transform techniques to get phase and magnitude information between the airfoil and shock motions for the various harmonics.

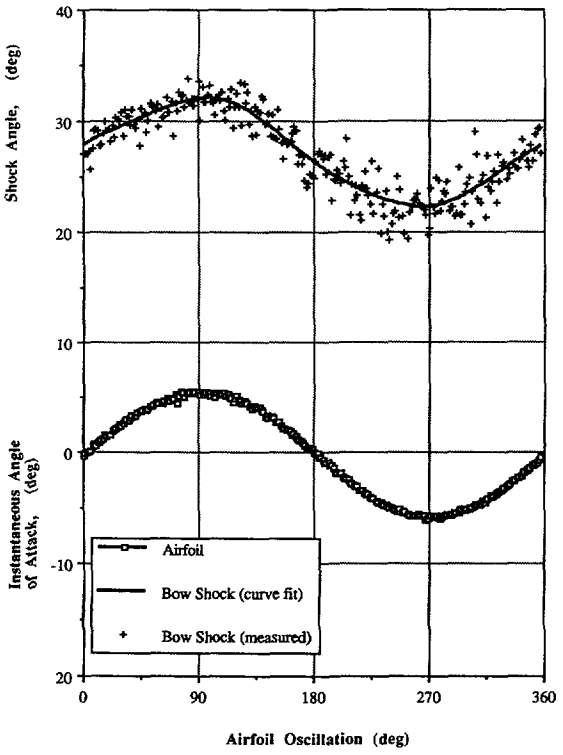

Fig. 9.

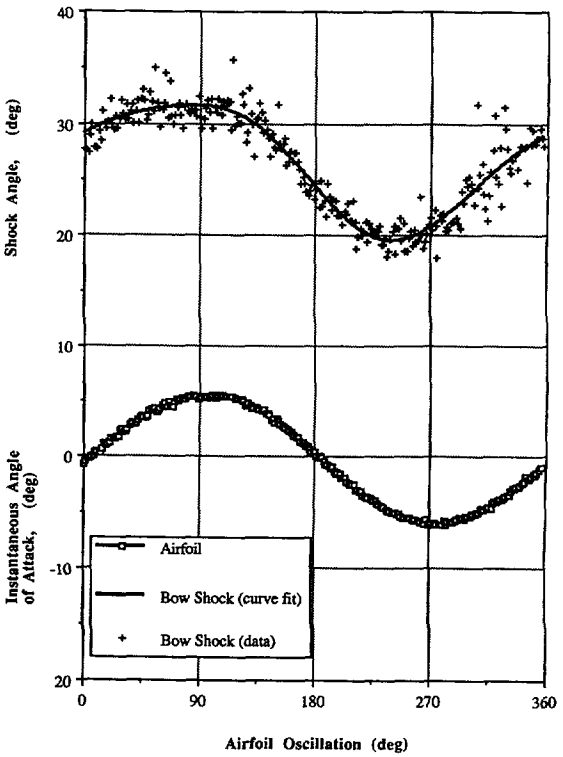

Fig. 10.

Fig. 9. — Bow shock location and airfoil angle of attack *vs.* Drive system location $k = 0.1$. Mach number = 2.81.

Fig. 10. — Bow shock location and airfoil angle of attack *vs.* Drive system location $k = 0.64$. Mach number = 2.81.

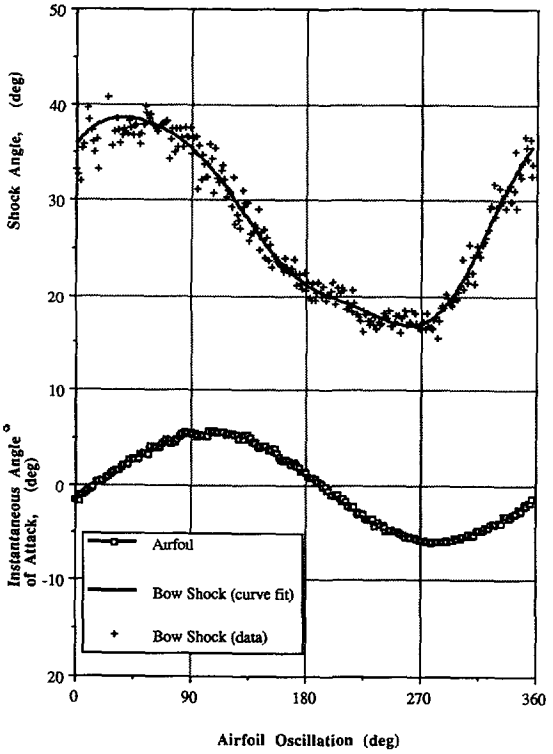

Fig. 11.

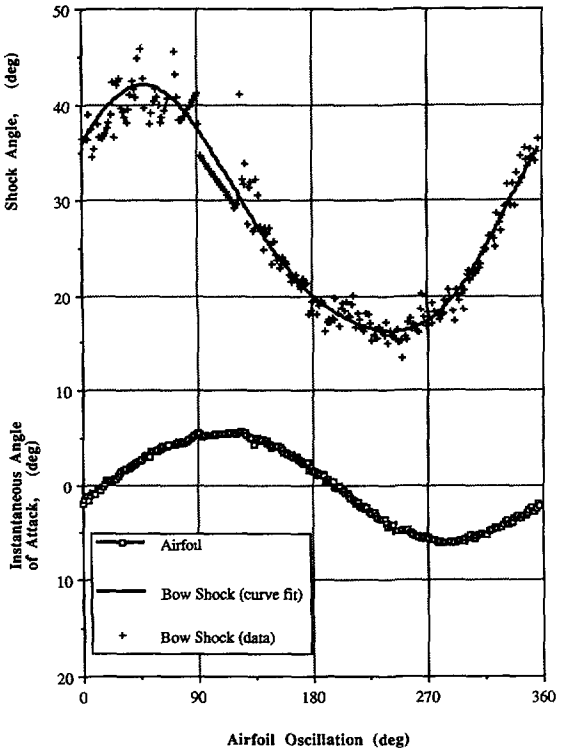

Fig. 12.

Fig. 11. — Bow shock location and airfoil angle of attack *vs.* Drive system location $k = 2.10$. Mach number = 2.81.

Fig. 12. — Bow shock location and airfoil angle of attack *vs.* Drive system location $k = 2.52$. Mach number = 2.81.

4. Results.

The experimental results for the wave angles measured for the supersonic and transonic flow conditions are now considered. The supersonic bow shock location as a function of airfoil location are presented with the reduced frequency as parameter. Also, analogous transonic chordwise normal shock data are presented. The results for the supersonic bow shock phenomena are shown in figures 9 through 15 with the transonic shock results presented in figures 16 through 18.

4.1 SUPERSONIC FLOW. — The instantaneous airfoil angle of attack, α, and the oblique shock angle, β, for a complete oscillation cycle with an inlet Mach number of 2.18 and reduced frequencies of 0.10, 0.64, 2.10, and 2.52 are presented in figures 9 through 12. Since the airfoil is symmetric, it is only necessary to consider the bow shock emanating from the lower surface. At low values of the reduced frequency, the shock motion is nearly sinusoidal and in phase with the airfoil motion. However, as the reduced frequency is increased, the shock motion becomes less sinusoidal and out of phase with the airfoil motion.

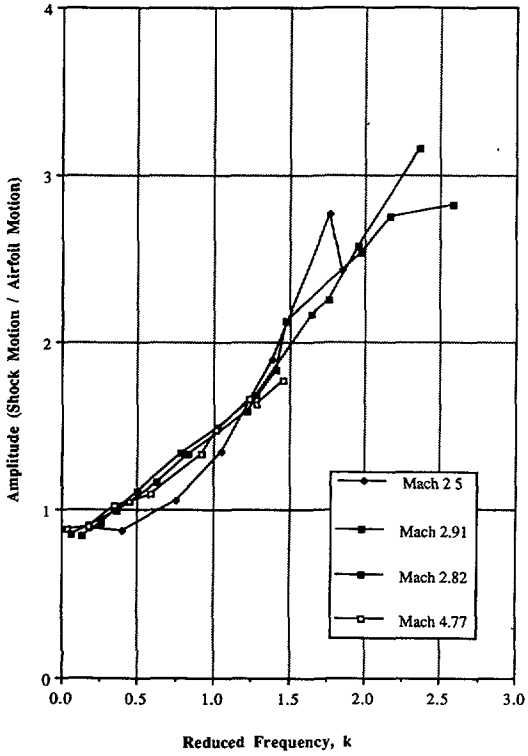

Fig. 13.

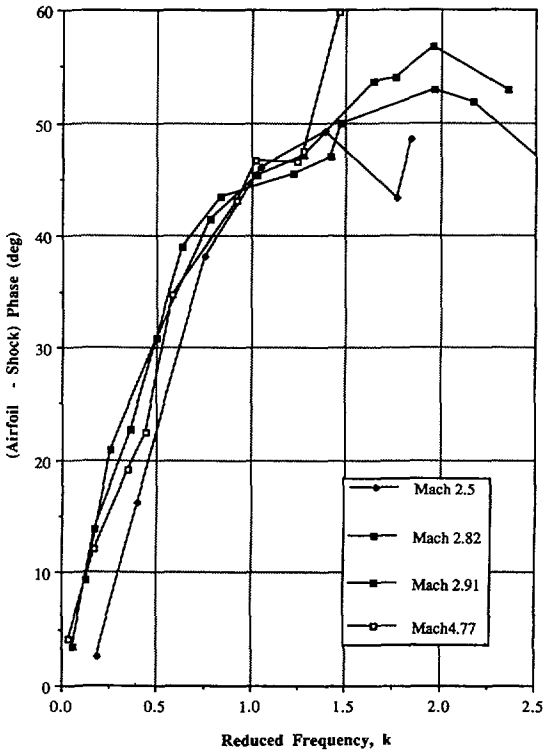

Fig. 14.

Fig. 13. — Amplitude ratio *vs.* reduced frequency, 1st harmonic.

Fig. 14. — Difference between airfoil and shock phase *vs.* reduced frequency, 1st harmonic.

The amplitude of the motion of the shock increases as the reduced frequency increases. This is demonstrated for the first harmonic data in figure 13 which shows the shock oscillation amplitude normalized with the airfoil amplitude as a function of the reduced frequency. At low reduced frequency values, the shock motion has slightly less amplitude of oscillation than the airfoil. However, as the reduced frequency is increased in value, the amplitude of the bow shock motion increases independent of the Mach number, for example at a reduced frequency of 2.0, the shock motion is approximately 2.5 times larger than the airfoil oscillation.

The phase difference between the first harmonic of the shock and airfoil motion as a function of the reduced frequency is shown in figure 14. At low reduced frequency values, the shock is in phase with the airfoil oscillation, as expected. As the reduced frequency increases, the shock motion begins to lag the motion of the airfoil, with this change linear to a reduced frequency of approximately 1.0 where the shock phase lag is 45°. At higher values of the reduced frequency, this phase lag becomes independent of the reduced frequency, with the shock lagging the airfoil by about 50° independent of the Mach number. Figure 15 shows the second harmonic phase of the shock motion relative to the first harmonic of the airfoil motion. The second harmonic phase starts at 180° out of phase with the blade motion at a quasi-steady condition. As k increases, the phase decreases in a linear fashion. The change in phase is relatively independent of Mach number and does not appear to flatten out at high values of reduced frequency.

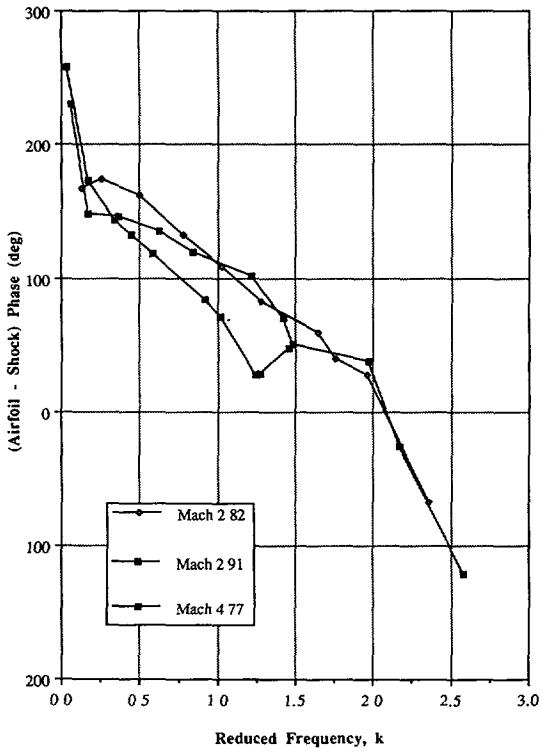

Fig. 15.

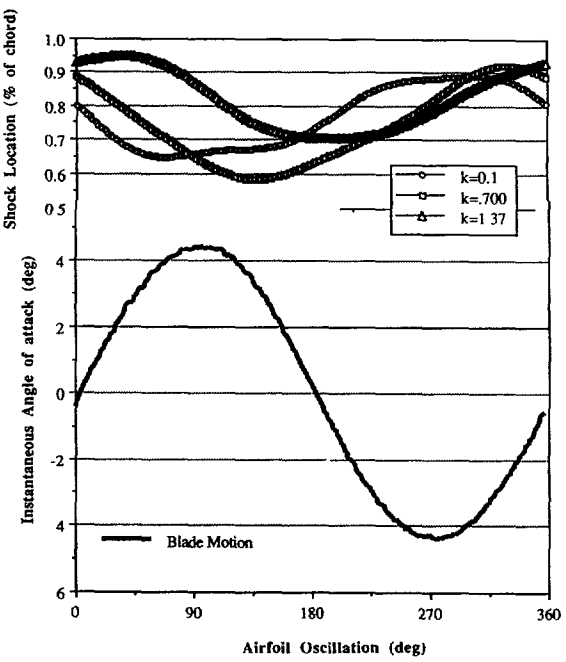

Fig. 16.

Fig. 15. — Difference between airfoil and shock phase *vs.* reduced frequency, 2nd harmonic shock, 1st harmonic airfoil.

Fig. 16. — Normal shock chordwise location *vs.* reduced frequency.

4.2 TRANSONIC FLOW SHOCK. — Transonic flow past the airfoil was generated by decreasing the Froude number until a normal hydraulic jump was observed near the trailing edge of the airfoil. Since the inlet flow is subsonic, a bow shock does not exist. Thus, it was not possible to measure the bow hydraulic jump to determine the inlet Froude number. A theoretical value of 0.9 based on aerodynamic conditions which provide the same shock formation was therefore utilized. As seen, the location of the shock changes significantly with reduced frequency.

The motion of the normal shock in terms of the shock instantaneous chordwise location on the airfoil surface together with the airfoil motion, with reduced frequency as parameter, is presented in figure 16. Figure 17 shows the effect of reduced frequency on the phase of the shock motion. The shock starts at 180° out of phase with the blade motion and decreases in a linear fashion at the rate of $50°*(\Delta k)$. The shock motion is 180° out of phase with the airfoil oscillation due to the fact that at low reduced frequency an increase in the angle of attack causes the normal shock to move to a more forward chordwise location. The inverse is true as the airfoil decreases it's angle of attack. At higher values of the reduced frequency, this phase difference decreases, with the shock motion lagging the airfoil motion.

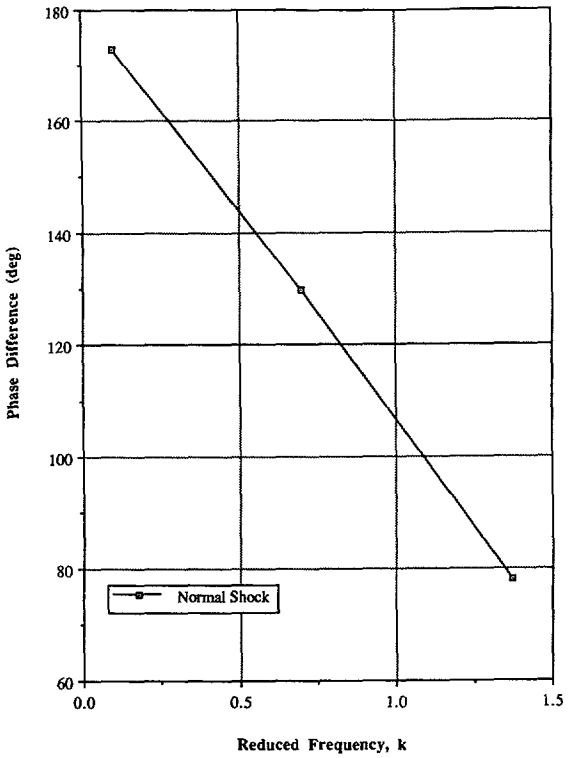

Fig. 17. — Difference between airfoil and normal shock phase *vs.* reduced frequency, 1st harmonic.

5. Summary and conclusions.

(1) The free surface water table provides an efficient and cost effective medium for studying oscillatory airfoil unsteady aerodynamics. However, correction of the hydraulic analogy is required to obtain valid quantitative bow shock data.

(2) The use of a computer based video enhancement system enabled acquisition and analysis of unsteady data on a real time basis and facilitated the recognition of the shock structure and motion.

(3) The magnitude and phase relationships for the bow shock are relatively independent of Mach number.

(4) The magnitude of oscillation of the bow shock is a strong function of the reduced frequency value, being of the same magnitude as the generating airfoil motion at low reduced frequency and 2.5 times larger than that of the airfoil at a reduced frequency of 2.0.

(5) The supersonic bow shock is in phase with the airfoil motion at low reduced frequency, lagging the airfoil motion as the reduced frequency is increased. This result is independent of the Mach number.

(6) The transonic normal shock location with relation to blade motion is linear and changes according to $50°*(\Delta k)$.

References

[1] KIELB R. E. and RAMSEY J. K., Flutter of a Fan Blade in Supersonic Axial Flow, *ASME Paper 88-GT-78* (June 1988).

[2] LANE F., Supersonic Flow Past an Oscillating Cascade with Supersonic Leading Edge Locus, *J. Aeronautical Sci.* **24** 65-66 (1957).

[3] SPARA K. M. and FLEETER S., Supersonic Turbomachine Rotor Flutter Control by Aerodynamic Detuning, *AIAA 89-2685* (July 1989).

[4] PREISWERK E., Application of the Methods of Gas Dynamics to Water Flows with Free Surface Part I Flows with no Energy Dissipation, *NACA TM No. 934* (1940) ; Part II Flows with Momentum Discontinuities (Hydraulic Jump) *NACA TM No. 935* (1940).

[5] ORLIN W. J., LINDNER N. J. and BITTERLY J. G., Application of the Analogy Between Water Flow with a Free Surface and Two-dimensional Compressible Gas Flow, *NACA TN-1185* (February 1947).

[6] IPPEN A. T. and HARLEMAN D. R. F., Studies on the Validity of the Hydraulic Analogy to Supersonic Flow, *Air Force Tech. Rep. No. 5985* Part I (May 1950) ; Part II (October 1950).

[7] CROSSLEY H. E. Jr. and HARLEMAN D. R. F., Studies on the Validity of the Hydraulic Analogy to Supersonic Flow, *Air Force Tech. Rep. No. 5985* Part V (December 1952).

[8] MACH E., Photography of Projectile Phenomena in Air, *Sitzungber. Wiener Akad.* **95** (1887) 164.

[9] JOUGUET E., Some Problems in General Hydrodynamics, *J. Math. Pures Appl.* **31** (1920) Series 8.

[10] BLACK J. and MEDIRATTA O. P., Supersonic Flow Investigations with a Hydraulic Analogy Water Channel, *Aeronaut. O.* **II** (February 1951).

[11] LAMB H., Hydrodynamics (Cambridge University Press 6th Ed. 1932).

[12] IPPEN A. T. and HARLEMAN D. R. F., Verification of Theory for Oblique Standing Waves, *Trans. Am. Soc. Civ. Eng.* **121** (1956).